Journal of Science and Technology – Engineering and Technology for Sustainable Development
Volume 36, Issue 4, October 2026, 000–000

Influence of $Sr(Sn_{0.5}Zr_{0.5})O_3$ Modification on Phase Structure and Electrical Response of $(Bi_{0.5}Na_{0.5})TiO_3$–$0.07BaTiO_3$ Ceramics near the Morphotropic Phase Boundary

Pham Thao Nhi[1], Ta Thi Thu Yen[1], Nguyen Ngoc Minh[1], Nguyen Thi Thao[1], Thi Hinh Dinh[2], Vu Diem Ngoc Tran [1,*]

[1]School of Materials Science and Engineering, Hanoi University of Science and Technology, Ha Noi, Vietnam
[2]Faculty of Materials Science and Engineering, Phenikaa University, Ha Noi, Vietnam
[*]Corresponding author email: ngoc.tranvudiem@hust.edu.vn

Abstract

$(Bi_{0.5}Na_{0.5})TiO_3$–$0.07BaTiO_3$–$xSr(Sn_{0.5}Zr_{0.5})O_3$ (abbreviated as BNT–7BT–xSSZ) ceramics were fabricated via a conventional solid-state reaction method with x in the range 0–0.05, where 1 wt.% Li_2CO_3 was introduced to reduce the sintering temperature to approximately 1050 °C. All samples maintain the coexistence of R3c and P4bm phases and exhibit typical relaxor-type behavior. Among all compositions, x equal 0.01 exhibits the best electromechanical performance, with the highest strain (S_{max} approximately 0.23 % at 60 kV/cm) and a corresponding high dynamic piezoelectric coefficient (d_{33}^* approximately 385 pm/V). This behavior is attributed to a relatively higher P4bm fraction within the morphotropic phase boundary region, which enhances polar nano-region dynamics and facilitates reversible polarization under an applied electric field. With increasing dopant content, the electromechanical response gradually decreases due to reduced polarization and strain activity, while the relaxor characteristics are maintained across all compositions. These results demonstrate that $Sr(Sn_{0.5}Zr_{0.5})O_3$ (SSZ) doping is an effective strategy to tune the structure–property relationship in BNT-based ceramics for electromechanical applications.

Keywords: BNBT, lead-free, piezoelectric, ceramic, SSZ.

1. Introduction

Lead zirconate titanate (Pb(Zr, Ti)O_3, PZT) piezoelectric ceramics have been widely used in actuators, sensors, and transducers due to their excellent piezoelectric and dielectric properties [1-4]. However, the intrinsic toxicity of lead and increasingly strict environmental regulations have driven intensive research toward the development of lead-free dielectric and piezoelectric materials with comparable performance [2, 5, 6]. Among various lead-free candidates, systems exhibiting morphotropic phase boundary (MPB)-like characteristics, such as BNT-based ceramics, have attracted particular attention.

$(Bi_{0.5}Na_{0.5})TiO_3$ (BNT) is considered one of the most promising lead-free materials due to its high saturation polarization ($P_{max} \approx 40$ μC/cm^2) and relatively high characteristic temperature [7]. However, pure BNT suffers from several drawbacks, including a high coercive field, large remanent polarization, and relatively low breakdown strength, resulting in wide hysteresis loops and limited recoverable energy density. To overcome these limitations, the formation of solid solutions with $BaTiO_3$ (BT) has been widely adopted. In the (1−*x*)BNT–*x*BT system, the morphotropic phase boundary appears near *x* approximately 6–7 mol%, where rhombohedral and tetragonal/pseudocubic phases coexist [8, 9]. This structural instability facilitates polarization rotation and enhances electromechanical response. However, despite the advantages of MPB, BNT–BT systems still exhibit relatively large remanent polarization, which limits the polarization difference ΔP and thus reduces energy storage performance. Therefore, further modification is required to destabilize long-range ferroelectric order and promote relaxor behavior.

A-site substitution in BNT-based systems, such as Sr^{2+}, can weaken long-range ferroelectric order, reduce the temperature of maximum permittivity, and enhance relaxor characteristics [10, 11]. Meanwhile, B-site substitution using ions such as Zr^{4+} and Sn^{4+} can induce lattice expansion due to their larger ionic radii compared to Ti^{4+}, thereby disrupting long-range ferroelectric order and promoting relaxor behavior with slimmer *P–E* loops. While Zr^{4+} doping has been reported to facilitate electric-field-induced strain (S_{max}) and enhance dielectric response, Sn^{4+} substitution tends to weaken ferroelectric order and may contribute to improved breakdown strength (E_b) [12, 13]. In particular, co-doping at both A and B-sites enables simultaneous control of phase structure and local lattice distortion, offering a promising approach to optimizing polarization

p-ISSN 3093-3242
e-ISSN 3093-3579
https://doi.org/10.51316/jst.xxx.etsd.xxxx.xx.x.x
Received: Apr 7, 2026; Revised: Jun 9, 2026;
Accepted: Jun 29, 2026; Online: Jul 28, 2026

difference, breakdown strength, and energy storage efficiency [14].

In this work, $(Bi_{0.5}Na_{0.5})TiO_3$–$0.07BaTiO_3$–xSr$(Sn_{0.5}Zr_{0.5})O_3$ (BNT–7BT–xSSZ, x = 0–0.05) ceramics were prepared near the MPB region to exploit phase coexistence and polarization instability. A specific Sr:Zr:Sn ratio of 2:1:1 was employed to explore potential synergistic effects between A-site and B-site substitutions. Sr incorporation is expected to suppress long-range ferroelectric order, while Zr and Sn contribute to lattice distortion and promote relaxor behavior.

In addition to compositional modification, reducing the sintering temperature without deteriorating functional properties is also of great importance for practical applications of ceramic materials. One effective approach is to introduce low-melting-point additives, such as Li_2CO_3, Li_2O, or CuO, which can form a transient liquid phase during sintering [15]. In this work, a small amount of Li_2CO_3 (1 wt.%) was introduced as a sintering aid to promote densification via a liquid-phase-assisted mechanism, thereby reducing the sintering temperature to below 1100 °C. This approach not only helps to reduce energy consumption and processing costs but also mitigates the volatilization of alkali elements, thereby improving the compositional stability of the ceramics.

The effects of dopant concentration on phase structure, microstructure, dielectric properties, ferroelectric behavior (*P–E*), strain response (*S–E*), and energy storage performance (W_{rec}, η) are systematically investigated. The relationship between phase evolution, relaxor characteristics, and functional properties is discussed to provide insights into the design of high-performance lead-free functional ceramics.

2. Experimental Procedure

In this study, $(Bi_{0.5}Na_{0.5})TiO_3$–$0.07BaTiO_3$–xSr$(Sn_{0.5}Zr_{0.5})O_3$ (BNT–7BT–xSSZ, x = 0–0.05) ceramics were synthesized by the conventional solid-state reaction method. The raw materials, Bi_2O_3, Na_2CO_3, $BaCO_3$, TiO_2, SrO, SnO_2, ZrO_2, and Li_2CO_3 (all greater than 99 % purity), were weighed according to the designed stoichiometric ratios and ball-milled in 96 % ethanol at a ball-to-powder weight ratio of 10:1 for 24 h. The resulting slurry was dried at 80 °C for 4 h and then calcined at 850 °C for 3 h to achieve phase formation. After calcination, 1 wt.% Li_2CO_3, used as a sintering aid, was added to the powder and mixed with ethanol to promote liquid-phase formation during sintering and reduce the sintering temperature, and then dried. The dried powders were then mixed with a 5 wt.% polyvinyl alcohol (PVA) solution as a binder and uniaxially pressed into pellets with a diameter of 12 mm and an area of 113.1 mm^2 under a pressure of 150 MPa using a hydraulic press. To minimize the volatilization of Na^+ and Bi^{3+}, the samples were sintered using the buried powder method. Before sintering, the samples were heated at 550 °C for 2 h to remove the PVA binder and then sintered at 1050 °C for 2 h. After sintering, silver electrodes were applied to both surfaces of the samples, followed by annealing at 700 °C for 3 h to ensure the formation of well-adhered electrode layers. The silver-electroded samples were poled in silicone oil at 90 °C under an electric field of 40 kV/cm for 30 min.

The phase structure was analyzed by X-ray diffraction (XRD) using Aeris with CuK_α radiation (λ = 1.5406 Å) for unpoled and poled samples. The GSAS-II software was used for Rietveld fitting to determine the phase composition of unpoled samples. The microstructure was observed using scanning electron microscopy. The dielectric properties, including dielectric constant (ε_r) and dielectric loss ($tan\delta$) as a function of temperature, were measured using a Hewlett-Packard impedance analyzer on silver-electroded samples. The ferroelectric hysteresis loops (*P–E* loops) and the electric-field-induced strain (*S–E* curves) were measured using the Sawyer-Tower circuit method under a maximum electric field of 60 kV/cm. The piezoelectric constant (d_{33}) was determined using a PIEZO METER (IACAS, Model ZJ–6B) with a ×0.1 range scale and a ±5 % accuracy spanning 2 to 40 pC/N. Based on the *P–E* hysteresis loops, the stored energy density (W_{rec}), total energy density (W), and energy storage efficiency (η) of the BNT–7BT–xSSZ ceramics were calculated according to the following equations [13]:

$$W_{rec} = \int_{Pr}^{P_{max}} E\, dP \quad (1)$$

$$W = \int_{0}^{P_{max}} E\, dP \quad (2)$$

$$\eta = \frac{W_{rec}}{W_{store}} \times 100\% \quad (3)$$

3. Results and Discussion

The X-ray diffraction patterns of all samples exhibit the typical perovskite structure, as shown in Fig. 1, indicating that the dopant ions are effectively incorporated into the crystal lattice. At higher doping concentrations (x = 0.04–0.05), a weak secondary peak appears at 2θ approximately 30°, which is tentatively assigned to $Na_{0.5}Bi_{0.45}Ti_4O_{15}$ phase based on JADE software matching and previous reports [13]. With increasing dopant concentration, the main diffraction peaks tend to shift toward lower 2θ angles, suggesting lattice expansion due to the larger ionic radii of the dopant ions compared to the host ions. Specifically, the ionic radii at the A-site are Bi^{3+} (1.03 Å), Na^+ (1.02 Å), Ba^{2+} (1.42 Å), and Sr^{2+} (1.26 Å), while at the B-site, the ionic radii are Ti^{4+} (0.61 Å), Sn^{4+} (0.71 Å), and Zr^{4+} (0.84 Å).

In the undoped BNT–7BT sample (x = 0), the splitting of the (111) and (200) diffraction peaks indicates the coexistence of rhombohedral (R3c) and

tetragonal-like relaxor (P4bm) phases [16]. This phase coexistence is a characteristic feature of the morphotropic phase boundary (MPB) in the BNT–BT system. As the dopant concentration increases, the XRD peak splitting gradually decreases, indicating enhanced structural disorder within the lattice [17]. At x equal 0.04, the split peaks nearly merge into a single peak, suggesting that the structure approaches a pseudo-cubic state. For the x equal 0.02 sample, the XRD peaks of the unpoled specimen shift anomalously toward higher 2θ angles, indicating a slight lattice contraction. This phenomenon may be associated with local lattice distortion caused by dopant incorporation.

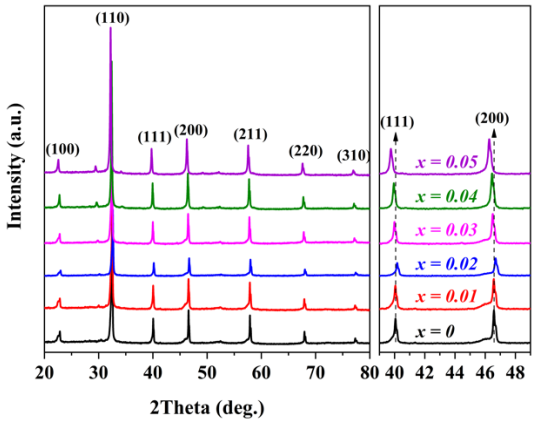

Fig. 1. XRD patterns of the BNT–7BT–xSSZ samples

After poling, the external electric field helps reorient the domains and alter the lattice parameters. The lattice generally expands, as evidenced by the leftward shift of the diffraction peaks. However, for the x equal 0.05 sample, the lattice parameter decreases after poling, indicating an anomalous structural response compared with the other compositions. The origin of this behavior is not yet fully understood but may be related to the increased structural complexity associated with high SSZ concentrations. To analyze the crystal structure in detail, the XRD data of the unpoled samples were refined using the Rietveld method with a two-phase model consisting of R3c and P4bm, as presented in Fig. 2 and Table 1. The low values of R_{wp} (below 6 %) and χ^2 (1.66–2.16) confirm that the two-phase model (R3c+P4bm) is reliable. The refinement results indicate that all samples exhibit the coexistence of these two phases, with phase fractions fluctuating around 40–60 %, suggesting that the material system consistently resides within an extended MPB region. The competition between these two phases reduces the energy barrier for polarization rotation and electric-field-induced phase transitions, thereby directly influencing the electrical properties of the material [18]. The variation in dopant concentration primarily adjusts the phase fraction between R3c and P4bm rather than inducing a complete phase transition. At x equal 0.01, the P4bm phase dominates (~56 %), indicating strong relaxor behavior, while at x equal 0.04, the phase ratio R3c:P4bm approximately 1:1 corresponds to a balanced phase state within the MPB. Substitution by Sr^{2+}, Zr^{4+}, and Sn^{4+} ions increases lattice disorder and promotes the formation of polar nanoregions (PNRs). This contributes to maintaining the relaxor state and controlling the phase proportion within the system [8, 11, 19].

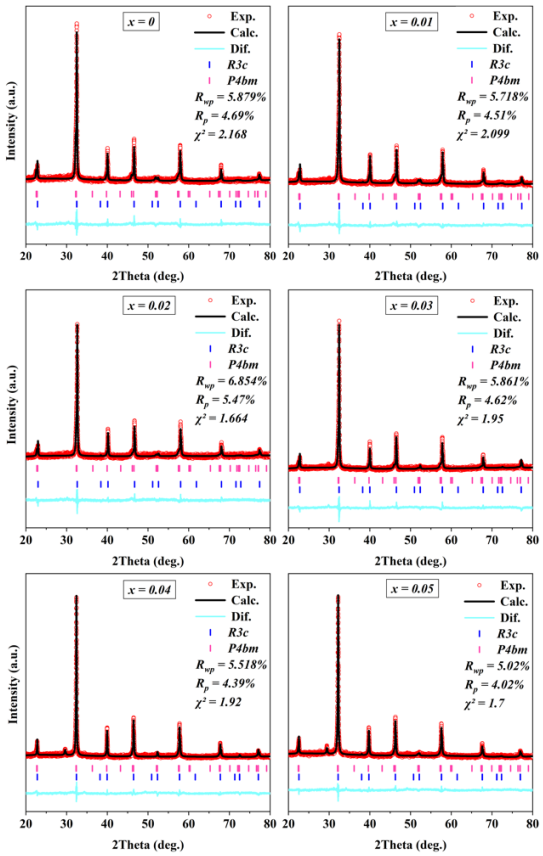

Fig. 2. Rietveld refinement of XRD patterns for unpoled BNT–7BT–xSSZ samples

Fig. 3 shows the microstructure and grain-size distributions of the BNT–7BT–xSSZ ceramics. The average grain size generally decreases with increasing SSZ content up to x equal 0.03, followed by a pronounced increase at x equal 0.04 and a subsequent decrease at x equal 0.05. The x equal 0.04 composition exhibits the largest average grain size and the broadest grain-size distribution, indicating enhanced grain-growth behavior and increased microstructural heterogeneity. In contrast, the x equal 0.05 sample shows a reduction in grain size accompanied by a wider dispersion of grain dimensions. These results indicate that SSZ addition affects the microstructural evolution of the BNT–7BT ceramics, although no monotonic dependence of grain size on dopant concentration was observed.

Table 1. Refined lattice parameters, phase fractions, and refinement indicators obtained from Rietveld analysis of BNT–7BT–xSSZ ceramics

x	Phase	Phase fraction (wt%)	a (Å)	c (Å)	R_{wp} (%)	R_p (%)	χ^2
0	R3c	54.46(31)	5.5152(5)	13.5141(8)	5.879	4.69	2.168
	P4bm	45.54(31)	5.5361(9)	3.9514(3)			
0.01	R3c	44.47(32)	5.5173(4)	13.5187(7)	5.718	4.51	2.099
	P4bm	55.53(32)	5.5315(8)	3.9471(3)			
0.02	R3c	54.10(42)	5.5184(5)	13.5183(9)	6.854	5.47	1.664
	P4bm	45.90(42)	5.5350(9)	3.9471(5)			
0.03	R3c	56.76(38)	5.5243(3)	13.5414(9)	5.861	4.62	1.95
	P4bm	43.24(38)	5.5375(9)	3.9517(4)			
0.04	R3c	48.43(39)	5.5309(4)	13.5436(7)	5.518	4.39	1.92
	P4bm	51.57(39)	5.5329(7)	3.9326(6)			
0.05	R3c	56.29(37)	5.5282(4)	13.5368(8)	5.02	4.02	1.7
	P4bm	43.71(37)	5.5317(8)	3.9371(6)			

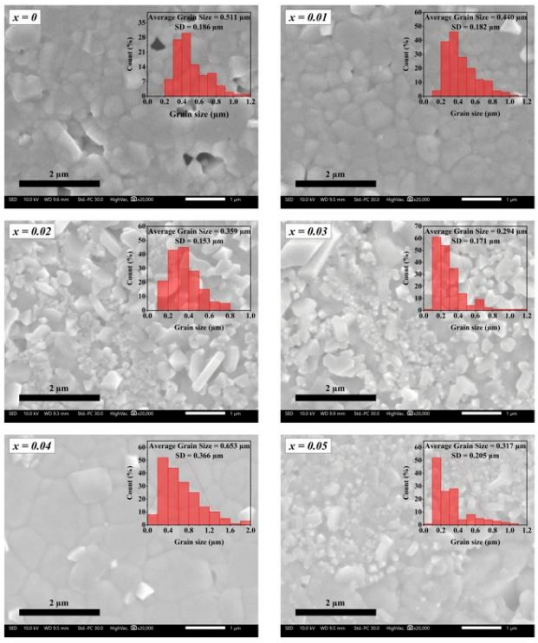

Fig. 3. Microstructure of BNT–7BT–xSSZ samples

The dielectric properties of the poled samples are shown in Fig. 4. The depolarization temperature (T_d) is around 110 °C before poling and slightly decreases to approximately 100 °C after poling. This minor variation suggests that the polarized state of the material is relatively stable. The dielectric constant reaches its maximum value at x equal 0.04 over the entire investigated temperature range (Fig. 4a), indicating that this composition is optimal from the viewpoint of dielectric performance. At this composition, the phase ratio R3c: P4bm approximately 1:1 corresponds to a balanced phase state within the MPB region. The long-range ferroelectric order in BNT–BT ceramics is disrupted, creating smaller polar nanoregions. This distortion enhances the ergodic relaxor behavior of the material and facilitates reversible polarization response under an external electric field, thereby improving its dielectric properties [16].

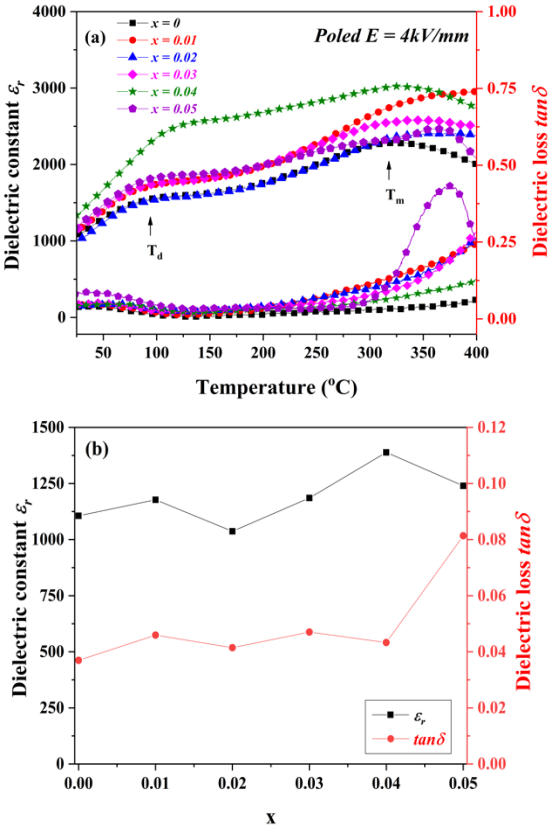

Fig. 4. Dielectric properties as a function of temperature (a) and dielectric properties at room temperature (b) of BNT–7BT–xSSZ poled samples

In contrast, the x equal 0.02 sample exhibits the lowest ε_r value. This is consistent with the XRD results, which indicate lattice contraction, leading to a reduction in spontaneous polarization and limiting the polarizability of the material. The dielectric loss ($tan\delta$) gradually decreases as the temperature increases from room temperature to approximately 250 °C and then rises sharply at higher temperatures (reaching about 25 % at 400 °C). At elevated temperatures, the formation of oxygen vacancies and free electrons can contribute to electrical conduction, resulting in a significant increase in dielectric loss.

The dielectric constant and dielectric loss at room temperature are shown in Fig. 4b. For the x equal 0.04 sample, the ε_r value reaches a maximum of 1300, while $tan\delta$ reaches 4 %. When the doping level is 0.05, the ε_r value decreases to 1092, and $tan\delta$ increases to approximately 8 %, which is higher than that of the other samples. This behavior may be associated with the increased conduction-related effects reflected by the elevated dielectric loss at high SSZ concentrations. Overall, the x equal 0.04 composition exhibits the most favorable dielectric response among all investigated compositions, suggesting its suitability for dielectric-related applications.

Fig. 5 shows the P–E hysteresis loops of the BNT–7BT–xSSZ ceramics with x equal 0, 0.01, 0.02, 0.03, 0.04, and 0.05, respectively. All samples exhibit slim P–E loops with a very low remanent polarization ($P_r \approx 2.8$ μC/cm^2) and a maximum polarization (P_{max}) of around 15 μC/cm^2, indicating typical relaxor-like behavior. However, a clear trend can be observed with increasing dopant concentration.

The P_{max} value increases significantly for the sample doped with x equal 0.01, then drops markedly at x equal 0.02. As the dopant concentration increases from x equal 0.03 to x equal 0.05, P_{max} shows a slight increase and exceeds that of the undoped sample, although the variation among these samples is relatively small. The highest P_{max} observed in the x equal 0.01 sample may be related to its relatively higher fraction of the P4bm phase compared to the other compositions. The presence of this phase enhances the mobility of PNRs under an external electric field, thereby increasing the maximum polarization. This interpretation is consistent with previous reports by L. Ling [20]. In contrast, the sharp decrease in P_{max} for the x equal 0.02 sample can be explained by the reduced lattice asymmetry. This reduction weakens the polarization response of the material, limiting the ability of dipoles to align effectively under the applied electric field, thus leading to a lower maximum polarization.

Fig. 6 shows the piezoelectric properties of the BNT–7BT–xSSZ ceramics, including the strain–electric field (S–E) behavior at different dopant concentrations. The undoped sample (x = 0) exhibits a typical butterfly-shaped curve characteristic of ferroelectric materials; however, the negative strain (S_{neg}) is very small, indicating the presence of a relaxor mechanism.

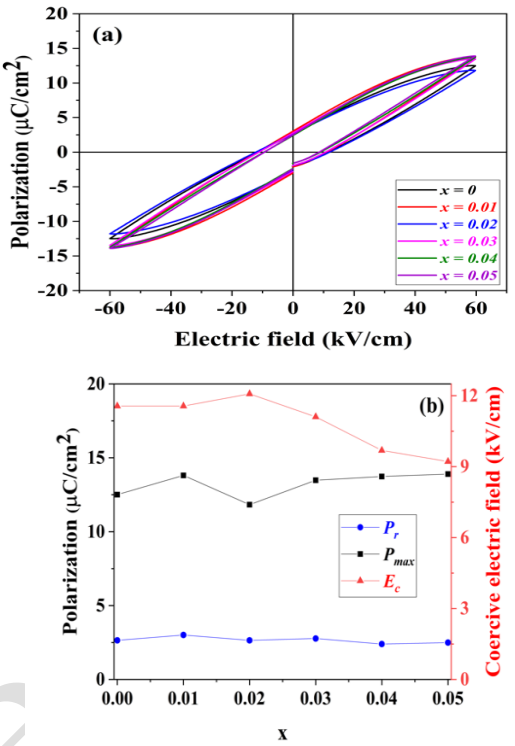

Fig. 5. Polarization vs electric field (a) and P_{max}, P_r, E_c (b) of BNT–7BT–xSSZ samples

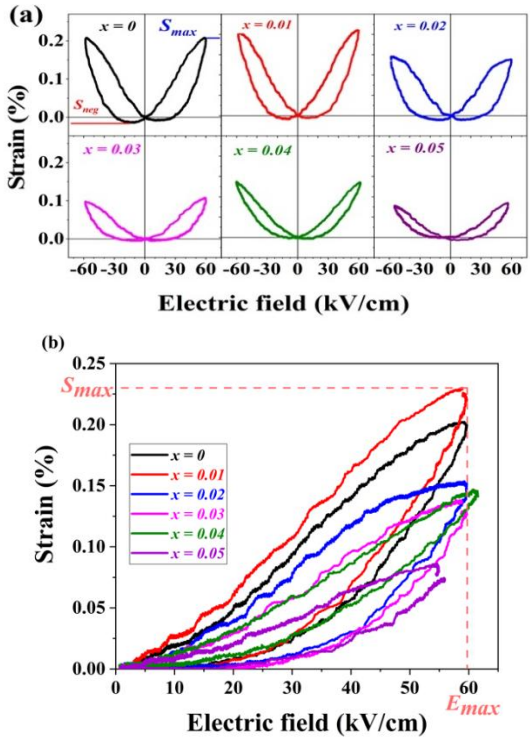

Fig. 6. Electric field-induced strain of BNT–7BT–xSSZ: bipolar (a) and unipolar (b)

When the dopant concentration increases to 0.01, the sample shows the highest maximum strain (S_{max}), while a small negative strain is still observed, suggesting that partial domain switching remains. At x equal 0.02, the strain decreases significantly to approximately 0.15 %, and S_{neg} remains noticeable, indicating a reduced electromechanical response. For the x equal 0.03 sample, the negative strain nearly disappears, but the overall strain remains low (~0.10 %), suggesting a gradual transition toward a more stable relaxor state. At x equal 0.04, the S–E curve becomes a fully slim loop, and the strain increases again (~0.14 %), indicating clear ergodic relaxor behavior, in which PNRs can reversibly reorient under an external electric field, leading to enhanced induced strain. For the x equal 0.05 sample, the strain curve becomes asymmetric, with the pinch point no longer centered at zero electric field, and the strain decreases sharply (~0.075 %). In BNT-based ceramics, the field-induced strain is strongly related to domain switching and relaxor–ferroelectric phase transformation [21]. The dopants may generate defect complexes and oxygen vacancies that pin domain walls and create internal electric fields, resulting in asymmetric bipolar strain loops. Furthermore, the suppression of the electric-field-induced phase transition reduces the reversible polarization switching, thereby decreasing the achievable strain response. This behavior may be associated with increased dielectric loss and the distortion of the P–E and S–E loops at high SSZ concentrations.

Table 2. Electromechanical properties of BNT–7BT–xSSZ ceramics

x	d_{33} (pC/N)	d_{33}^* (pm/V)	W_{total} (J/cm^3)	W_{rec} (J/cm^3)	η (%)
0	5	339	0.47	0.24	50.60
0.01	5	385	0.41	0.25	61.77
0.02	3	257	0.45	0.22	48.35
0.03	1	231	0.50	0.25	51.12
0.04	3	238	0.49	0.27	56.14
0.05	2	154	0.48	0.27	56.43

Table 2 presents the values of S_{max} and E_{max} obtained from the unipolar S–E loops, from which the d_{33}^* coefficient is calculated. The results show that the d_{33}^* value reaches its maximum in the x equal 0.01 sample (~385 pm/V), which is significantly higher than those of the other samples and corresponds to the highest maximum strain (S_{max}), indicating that a small amount of doping can effectively enhance the electromechanical response of the material under an external electric field. This improvement may be associated with a favorable coexistence of R3c and P4bm phases, where the relatively higher P4bm fraction facilitates the reorientation of PNRs and enhances reversible polarization under an external electric field. As the dopant concentration increases from x equal 0.02 onward, the d_{33}^* value gradually decreases, reaching its lowest value in the x equal 0.03 sample, which may be associated with a transition toward a more pronounced relaxor state and reduced spontaneous polarization. At x equal 0.04, the d_{33}^* value shows a slight recovery, suggesting a modest improvement in strain response, possibly due to changes in the phase fraction within the relaxor system. However, at x equal 0.05, the d_{33}^* value drops sharply to approximately 150 pm/V, which may be associated with increased dielectric loss and the degradation of electromechanical response at high SSZ concentrations. The piezoelectric coefficient d_{33} and the effective piezoelectric coefficient d_{33}^* show similar trends. However, the measured d_{33} values remain in the range of only 1–5 pC/N, which is significantly lower than those typically reported for the BNT–7BT system in previous studies [8, 16] (around 200 pC/N). This discrepancy can be attributed to the relaxor nature of the material system investigated in this work. In relaxor materials, the polarization induced under an external electric field mainly originates from the temporary reorientation of PNRs. Once the external field is removed, these regions tend to revert to their original random state, resulting in a very low remanent polarization and consequently a low d_{33} value. Overall, the x equal 0.01 composition exhibits the best electromechanical performance owing to its superior strain response and dynamic piezoelectric coefficient, indicating its potential for actuator-related applications.

The energy storage properties were calculated from the P–E loops and presented in Table 2. The recoverable energy density (W_{rec} ≈ 0.22–0.27 J/cm^3) remains relatively low despite the low P_r, mainly due to the limited P_{max} values. The energy storage efficiency reaches its maximum value of 62 % at x = 0.01, indicating the most favorable balance between recoverable energy density and hysteresis loss among the investigated compositions.

4. Conclusion

In this study, $(Bi_{0.5}Na_{0.5})TiO_3$–$0.07BaTiO_3$–$x Sr(Sn_{0.5}Zr_{0.5})O_3$ (BNT–7BT–xSSZ, x = 0–0.05) ceramics were successfully fabricated via a conventional solid-state reaction method, where the addition of 1 wt.% Li_2CO_3 enabled densification at a reduced sintering temperature of 1050 °C. XRD and Rietveld refinement analyses confirmed the coexistence of R3c and P4bm phases in all compositions, indicating that the investigated system remains within an extended morphotropic phase boundary region. SSZ incorporation effectively tailors the phase fraction and consequently modulates the functional properties of the ceramics.

The BNT–7BT–xSSZ system exhibits two distinct optimal responses depending on the targeted property. The x equal 0.04 composition shows the highest dielectric constant, which is associated with a nearly balanced R3c/P4bm phase coexistence within the MPB region, favoring polarization stability. In contrast,

the x equal 0.01 composition exhibits the best electromechanical performance, including the highest polarization, maximum strain response (S_{max} approximately 0.23 % at E equal 60 kV/cm), highest dynamic piezoelectric coefficient (d_{33}^* approximately 385 pm/V), and enhanced energy storage efficiency (η approximately 62%). This behavior is attributed to a favorable coexistence of R3c and P4bm phases with a relatively higher P4bm fraction, which enhances PNRs dynamics and facilitates reversible polarization under an applied electric field.

With increasing SSZ content beyond x equal 0.01, the electromechanical response gradually decreases due to reduced polarization and strain activity, while retaining relaxor behavior across all compositions. Overall, the x equal 0.01 composition demonstrates optimal electromechanical performance, making SSZ-modified BNT–7BT ceramics promising candidates for lead-free actuator applications. The dielectric maximum at x equal 0.04 further suggests potential for dielectric-related applications.

Acknowledgments

This work was supported by the Hanoi University of Science and Technology under the Grant T2024-PC099.

References

[1] P. Qiao, Y. Yang, Y. Wang, M. Zhang, P. Qian, J. Wang, and J. Zhang, Enhanced electromechanical performance of PSZT–PMS–PFW through morphotropic phase boundary design and defect engineering, Journal of Materials Chemistry C, vol. 11, no. 34, pp. 11631–11642, Jul. 2023. https://doi.org/10.1039/d3tc01433a

[2] G. Wang, Z. Lu. Y. Li, L. Li, H. Ji, A. Feteira, D. Zhou, D. Wang, S. Zhang, and I. M. Reaney, Electroceramics for high-energy density capacitors: current status and future perspectives, Chemical Reviews, vol. 121, no. 10, pp. 6124–6172, May 2021. https://doi.org/10.1021/acs.chemrev.0c01264

[3] A. Zhang, Z. Li, W. Yang, Z. Man, L. Zheng, C. H. Park, and G. Li, Enhanced electromechanical properties and thermal stability of PMnN–PZT piezoelectric ceramics near the MPB, Ceramics International, vol. 51, iss. 26, part B, pp. 49276–49284, Nov. 2025. https://doi.org/10.1016/j.ceramint.2025.08.169

[4] G. H. Haertling, Hot-pressed (Pb,La)(Zr,Ti)O_3 ferroelectric ceramics for electrooptic applications, Journal of the American Ceramic Society, vol. 54, iss. 1, pp. 1–11, Jan. 1971. https://doi.org/10.1111/j.1151-2916.1970.tb12105.x-i1

[5] J. Rödel, W. Jo, K. T. P. Seifert, E-M. Anto, T. Granzow, and D. Damjanovic, Perspective on the development of lead-free piezoceramics, Journal of the American Ceramic Society, vol. 92, iss. 6, pp. 1153–1177, Jun. 2009. https://doi.org/10.1111/j.1551-2916.2009.03061.x

[6] T. H. Dinh, V. D. N. Tran, T. L. Manh, and J-S. Lee, Effects of $BaZrO_3$ on the phase evolution and energy storage capacities of BNT-based lead-free dielectric ceramics, Journal of Physics and Chemistry of Solids, vol. 198, Art. no. 112462, Mar. 2025. https://doi.org/10.1016/j.jpcs.2024.112462

[7] W. Zhu, A review: (Bi,Na)TiO_3 (BNT)-based energy storage ceramics, Journal of Materiomics, vol. 10, iss. 1, pp. 86–123, Jan. 2024. https://doi.org/10.1016/j.jmat.2023.05.002

[8] J. Zhao, N. Zhang, Y. Quan, G. Niu, W. Ren, Z. Wang, K. Zheng, Y. Zhao, and Z-G. Ye, Evolution of mesoscopic domain structure and macroscopic properties in lead-free $Bi_{0.5}Na_{0.5}TiO_3$–$BaTiO_3$ ferroelectric ceramics, Journal of Applied Physics, vol. 129, iss. 8, Feb. 2021. https://doi.org/10.1063/5.0035466

[9] V. D. N. Tran, Effect of $SrTi_{0.875}Nb_{0.1}O_3$ doping on energy storage density of lead-free $Bi_{0.5}Na_{0.5}TiO_3$–$BaTiO_3$-based piezoelectric ceramics, Journal of Science and Technology - Engineering and Technology for Sustainable Development, vol. 36, iss. 1, pp. 17–23, Mar. 2026. https://doi.org/10.51316/jst.188.etsd.2026.36.1.3

[10] T. H. Dinh, H. T. Hieu V. D. N. Tran, M. T. Le, and J-S. Lee, High energy density performance of BNT–ST piezoceramics by Al_2O_3 doping, in Processding ICERA, vol. 1610, pp. 331–336, Oct. 2025. https://doi.org/10.1007/978-3-032-03856-2_36

[11] V. D. N. Tran, A. Ullah, T. H. Dinh, and J-S Lee, Large field-induced strain properties of $Sr(K_{0.25}Nb_{0.75})O_3$-modified $Bi_{1/2}(Na_{0.82}K_{0.18})_{1/2}TiO_3$ lead-free piezoelectric ceramics, Journal of Electronic Materials, vol. 45, pp. 2627–2631, Mar. 2016. https://doi.org/10.1007/s11664-016-4445-1

[12] A. Rachakom, Effect of poling on piezoelectric and ferroelectric properties of $Bi_{0.5}Na_{0.5}Ti_{1-x}Zr_xO_3$ ceramics, Journal of Electroceramics, vol. 33, no. 1–2, pp. 105–110, Jun. 2014. https://doi.org/10.1007/s10832-014-9939-8

[13] Y. Pu, L. Zhang, Y. Cui, and M. Chen, High energy storage density and optical transparency of microwave-sintered homogeneous $(Na_{0.5}Bi_{0.5})_{(1-x)}Ba_xTi_{(1-y)}Sn_yO_3$ ceramics, ACS Sustainable Chemistry and Engineering, vol. 6, iss. 5, pp. 6102–6109, Mar. 2018. https://doi.org/10.1021/acssuschemeng.7b04754

[14] R. M. A. K. Manj, Optimization of switching charge and recoverable energy density mediated by structural transformation in Sr-substituted $BaNiO_3$ perovskites, RSC Advances, vol. 14, iss. 22, pp. 15791–15803, May 2024. https://doi.org/10.1039/d4ra01439a

[15] N. Ma, Low-temperature sintering of Li_2O-doped $BaTiO_3$ lead-free piezoelectric ceramics, Journal of Electroceramics, vol. 28, no. 4, pp. 275–280, May 2012. https://doi.org/10.1007/s10832-012-9730-7

[16] S. Supriya, A review on lead-free $Bi_{0.5}Na_{0.5}TiO_3$-based ceramics and films: Dielectric, piezoelectric, ferroelectric and energy storage performance,

Journal in Inorganic and Organometallic Polymers and Materials, vol. 32, no. 10, pp. 3659–3676, Jul. 2022. https://doi.org/10.1007/s10904-022-02418-6

[17] R. M. A. K. Manj, Optimization of switching charge and recoverable energy density mediated by structural transformation in Sr-substituted $BaNiO_3$ perovskites, RSC Advances, vol. 14, iss. 22, pp. 15791–15803, May 2024. https://doi.org/10.1039/d4ra01439a

[18] Q. Qiu, H. Wang, Y. Xu, X. Chen, X, Liu, Y. Zhou, Z. Lv, J. Sun, S. Zhang, H. Zhang, A. Manan, G. Liu, and Y. Yan, Achieving high electrostrain performance in BNT-based lead-free piezoelectric ceramics modified by $Sr(Sn_{0.5}Ta_{0.4})O_3$, Journal of the American Ceramic Society, vol. 108, iss. 8, Aug. 2025. https://doi.org/10.1111/jace.20595

[19] D. Yang, X. Wu, X. Lv, L. Wen, J. Jin, and J. Wu, Random fields-triggered strain enhancement in BNT-based materials, Journal of the European Ceramic Society, vol. 45, iss. 1, Art. no. 116805, Jan. 2025. https://doi.org/10.1016/j.jeurceramsoc.2024.116805

[20] X. Li, X. Hao, S. An, Y. Li, and Q. Zhang, Enhanced energy storage in Sn-doped sodium bismuth titanate lead-free relaxor ferroelectric ceramics, Journal of Materials Science: Materials in Electronics, vol. 33, no. 8, pp. 5265–5272, Feb. 2022. https://doi.org/10.1007/s10854-022-07714-y

[21] L. Li, M. Zhu, Q. Wei, M. Zheng, Y. Hou, and J. Hao, Ferroelectric P4mm to relaxor P4bm transition and temperature-insensitive large strains in $Bi(Mg_{0.5}Ti_{0.5})O_3$-modified $0.875Bi_{0.5}Na_{0.5}TiO_3$–$0.125BaTiO_3$ ceramics, Journal of the European Ceramic Society, vol. 38, iss. 4, pp. 1381–1388, Apr. 2017. https://doi.org/10.1016/j.jeurceramsoc.2017.12.022

[22] Y. Wang, P. Wang, L. Liu, Y. Wang, Y. Zhao, W. Tian, X. Liu, F. Zhu, and J. Shi, Defect dipole behaviors on the strain performances of bismuth sodium titanate-based lead-free piezoceramics, Materials, vol. 16, May 2023, Art. no. 4008. https://doi.org/10.3390/ma16114008